FEM analysis of Cosserat plates and shells based on some constitutive relations

Jacek Chróścielewski, Wojciech Witkowski[1]

Gdansk University of Technology,

Faculty of Civil and Environmental Engineering, Department of Structural Mechanics and Bridge Structures

80-233 Gdańsk, Narutowicza 11/12, Poland

Key words: Micropolar constants, nonlinear six-parameter shell theory, drilling rotation, constitutive equations

Abstract

We carry out further study of the constitutive laws for Cosserat plates developed by Altenbach and Eremeyev. In particular, we examine the problem of choice of the micropolar material coefficients. Requiring that the constitutive matrix is positive definite, we establish some bounds on values of micropolar constants. The constitutive relations for Cosserat plates have been implemented into formulation of shell finite elements developed within the framework of the statically and kinematically exact, nonlinear six-parameter shell theory. By the linear parametric-sensitivity analysis we study the influence of the micropolar material constants on the response of shell structure with orthogonal intersections of branches. Such structures can naturally be analyzed using the six-parameter shell theory. Having established the most influential coefficients, we show how these values affect the behavior of the structure in the nonlinear range of deformations.

1. Introduction

The idea of oriented medium is a mature subject. The paper by Cosserat brothers [1] established a landmark in developing the concept of the continuum with the microstructure. Forgotten in its times the Cosserat's work has been rediscovered anew in the fifties of the 20th century. For the historical outline one may refer to, for example, the books by Eringen [2] or Nowacki [3] or the paper by Altenbach et al. [4]. Despite its age, the Cosserat continuum still receives much attention in the literature. For example, Pietraszkiewicz and Eremeyev [5] discussed different strain measures that can be defined within the framework of Cosserat medium, Altenbach and Eremeyev [6] developed theory of Cosserat plates, Ramezani and Naghdabadi [7] generalized the notion of hypo-elasticity for the micropolar media.

This paper is a follow-up of our previous paper [8] where we studied the conditions of equivalence (and its implications) between the constitutive relations for micropolar plates obtained in [6] and those formulated for the statically and kinematically exact, nonlinear, six-parameter shell theory used, among others, in [9][10][11] [13] [12][14][15]. It was shown that both models are equivalent for some values of the constitutive parameters. Assuming the equivalence, we derived the formula for the constitutive coefficient α_t from the shell constitutive relation. It was shown that, under assumption of equivalence, α_t may be expressed as the function of Poisson's ratio ν alone i.e.

[1] corresponding author, wojwit@pg.gda.pl

$$\alpha_t = \frac{2-\nu}{1-\nu} \text{ under } N = \tfrac{1}{2}\sqrt{2} \tag{1}$$

Our numerical results presented in [1] enabled us to introduce the notion of α_t -locking within the FEM analysis. The α_t -locking is responsible for too stiff response due to large values of α_t .

In this paper we continue to analyze the Altenbach and Eremeyev plate model. Their constitutive relations are implemented into the framework of our CAM elements (see [10] for details). While our previous paper [1] has been concerned with the linear analysis, here we focus on the geometrically nonlinear analysis. Yet, one needs first to select properly the values of material coefficients. It is well-known however, see for instance [2], [17], [18], [19] and the literature cited there, that this is a problematic issue, especially for accuracy of experimental measurements. To properly select values of the micropolar material constants we examine the structure of constitutive matrix and study its conditioning by analyzing its eigenvalues. We present some bounds on the values of micropolar material coefficients that should be imposed to make the constitutive matrix positive definite. With the help of linear parametric-sensitivity analysis, we study the influence of some material parameters on the overall response of the structure in the linear analysis. As an example we study the thin-walled, simply supported channel beam, regarded as the union of plates, yet with orthogonal intersections. Based on the results we proceed with the geometrically nonlinear analysis and examine the response of the structure with different values of some material coefficients.

2. Problem statement

This section serves only as the statement of the problem and does not provide any new results. It comprises the most important theoretical assumptions that lead to the results from the previous paper [8].

2.1. Altenbach and Eremeyev model of Cosserat plate

The elastic strain energy density for a solid plate may be written as (cf. [6] eq. 11, see also [16])

$$\begin{aligned} 2\Phi(\boldsymbol{\varepsilon}) = \alpha_1 tr^2 \boldsymbol{E}_{\parallel} + \alpha_2 tr\boldsymbol{E}_{\parallel}^2 + \alpha_3 tr(\boldsymbol{E}_{\parallel}^T \boldsymbol{E}_{\parallel}) + \alpha_4 \boldsymbol{t}_N^0 \boldsymbol{E}\boldsymbol{E}^T \boldsymbol{t}_N^0 + \\ + \beta_1 tr^2 \boldsymbol{K}_{\parallel} + \beta_2 tr\boldsymbol{K}_{\parallel}^2 + \beta_3 tr(\boldsymbol{K}_{\parallel}^T \boldsymbol{K}_{\parallel}) + \beta_4 \boldsymbol{t}_N^0 \boldsymbol{K}\boldsymbol{K}^T \boldsymbol{t}_N^0 \end{aligned} \tag{2}$$

Here symbol $\parallel$ denotes tangent component of some tensor $\boldsymbol{X}$ i.e.

$$\boldsymbol{X}_{\parallel} \equiv \boldsymbol{X} - \boldsymbol{t}_N^0 \boldsymbol{X} \ , \ \boldsymbol{X} \equiv \boldsymbol{X}_{\parallel} + \boldsymbol{t}_N^0 \otimes \boldsymbol{x} \ , \ \boldsymbol{x} = \boldsymbol{t}_N^0 \boldsymbol{X} \tag{3}$$

The constitutive coefficients α_i and β_i are given by

$$\alpha_1 = \tilde{\lambda} h = \frac{E\nu}{1-\nu^2} h \ , \quad \tilde{\lambda} = \frac{2\mu\lambda}{2\mu+\lambda} = \frac{E\nu}{1-\nu^2} \ , \quad \mu = \frac{E}{2(1+\nu)} \ , \tag{4}$$

$$\alpha_2 = (\mu - \tfrac{1}{2}\kappa) h \ , \tag{5}$$

$$\alpha_3 = (\mu + \tfrac{1}{2}\kappa) h \ , \tag{6}$$

$$\alpha_4 = (\mu + \tfrac{1}{2}\kappa) h \ , \tag{7}$$

$$\beta_1 = \alpha h - (\mu - \tfrac{1}{2}\kappa) \frac{h^3}{12} \ , \tag{8}$$

$$\beta_2 = \beta h - \tfrac{1}{12}\tilde{\lambda} h^3 , \tag{9}$$

$$\beta_3 = \gamma h - \tfrac{1}{12}(2\mu + \tilde{\lambda}) h^3 , \tag{10}$$

$$\beta_4 = \gamma h . \tag{11}$$

In writing the relations (4) through (11) it is assumed that μ in relations 45 in [6] should read in fact $\mu \equiv \mu - \frac{1}{2}\kappa$, compare for instance [20] and [21]. The constants α_i and β_i are expressed by six material parameters: two engineering constants E, ν, the coupling number N, the characteristic length for bending l_b, the characteristic length for torsion l_t and the non-dimensional micropolar ratio Ψ. These latter 4 constants read:

$$N^2 = \frac{\kappa}{2\mu + \kappa} \Rightarrow \kappa = 2\mu \frac{N^2}{1 - N^2} , \; 0 < N < 1 , \tag{12}$$

$$l_b^2 = \frac{\gamma}{4\mu} \Rightarrow \gamma = 4\mu l_b^2 , \tag{13}$$

$$l_t^2 = \frac{\beta + \gamma}{2\mu} \Rightarrow \beta = 2\mu l_t^2 - \gamma , \tag{14}$$

$$\Psi = \frac{\beta + \gamma}{\alpha + \beta + \gamma} \Rightarrow \alpha = (\beta + \gamma)\left(\frac{1 - \Psi}{\Psi}\right) = 2\mu l_t^2 \left(\frac{1 - \Psi}{\Psi}\right), \; 0 < \Psi \le \frac{3}{2} . \tag{15}$$

Through (2) the following constitutive relations for force tensor and the moment tensor are arrived at

$$\mathbf{N} = \alpha_1 \boldsymbol{A} tr \boldsymbol{E}_{\|} + \alpha_2 \boldsymbol{E}_{\|}^T + \alpha_3 \boldsymbol{E}_{\|} + \alpha_4 \boldsymbol{E} \boldsymbol{t}_N^0 \otimes \boldsymbol{t}_N^0 \tag{16}$$

$$\mathbf{M} = \beta_1 \boldsymbol{A} tr \boldsymbol{K}_{\|} + \beta_2 \boldsymbol{K}_{\|}^T + \beta_3 \boldsymbol{K}_{\|} + \beta_4 \boldsymbol{K} \boldsymbol{t}_N^0 \otimes \boldsymbol{t}_N^0 \tag{17}$$

with $\boldsymbol{A} = \mathbf{1} - \boldsymbol{t}_N^0 \otimes \boldsymbol{t}_N^0$. After some manipulations (see Appendix in [1]) equations (16) and (17) may be rewritten in component form, suitable for numerical implementation

$$\begin{bmatrix} N^{11} \\ N^{22} \\ N^{12} \\ N^{21} \\ Q^1 \\ Q^2 \\ M^{11} \\ M^{22} \\ M^{12} \\ M^{21} \\ M^1 \\ M^2 \end{bmatrix} = \left[\begin{array}{cccccc|cccccc} \alpha_1 + \underline{\alpha_2} + \alpha_3 & \alpha_1 & 0 & 0 & 0 & 0 & & & & & & \\ \alpha_1 & \alpha_1 + \underline{\alpha_2} + \alpha_3 & 0 & 0 & 0 & 0 & & & & & & \\ 0 & 0 & \alpha_3 & \underline{\alpha_2} & 0 & 0 & & & & & & \\ 0 & 0 & \underline{\alpha_2} & \alpha_3 & 0 & 0 & & & & & & \\ 0 & 0 & 0 & 0 & \alpha_4 & 0 & & & & & & \\ 0 & 0 & 0 & 0 & 0 & \alpha_4 & & & & & & \\ \hline & & & & & & \beta_1 + \underline{\beta_2} + \beta_3 & \beta_1 & 0 & 0 & 0 & 0 \\ & & & & & & \beta_1 & \beta_1 + \underline{\beta_2} + \beta_3 & 0 & 0 & 0 & 0 \\ & & & & & & 0 & 0 & \beta_3 & \underline{\beta_2} & 0 & 0 \\ & & & & & & 0 & 0 & \underline{\beta_2} & \beta_3 & 0 & 0 \\ & & & & & & 0 & 0 & 0 & 0 & \beta_4 & 0 \\ & & & & & & 0 & 0 & 0 & 0 & 0 & \beta_4 \end{array}\right] \begin{bmatrix} \varepsilon_{11} \\ \varepsilon_{22} \\ \varepsilon_{12} \\ \varepsilon_{21} \\ \varepsilon_1 \\ \varepsilon_2 \\ \kappa_{11} \\ \kappa_{22} \\ \kappa_{12} \\ \kappa_{21} \\ \kappa_1 \\ \kappa_2 \end{bmatrix} \tag{18}$$

2.2. Six-parameter shell theory

Although the constitutive relations of the six-parameter shell theory are not used directly in the present study, let us briefly address them to proceed further with the notion of equivalence.

The constitutive relation

$$\begin{aligned} N^{11} &= C(\varepsilon_{11}+\nu\varepsilon_{22}) & M^{11} &= D(\kappa_{11}+\nu\kappa_{22}) \\ N^{22} &= C(\varepsilon_{22}+\nu\varepsilon_{11}) & M^{22} &= D(\kappa_{22}+\nu\kappa_{11}) \\ N^{12} &= C(1-\nu)\varepsilon_{12} & M^{12} &= D(1-\nu)\kappa_{12} \\ N^{21} &= C(1-\nu)\varepsilon_{21} & M^{21} &= D(1-\nu)\kappa_{21} \\ Q^{1} &= \tfrac{1}{2}\alpha_s C(1-\nu)\varepsilon_{1} & M^{1} &= \alpha_t D(1-\nu)\kappa_{1} \\ Q^{2} &= \tfrac{1}{2}\alpha_s C(1-\nu)\varepsilon_{2} & M^{2} &= \alpha_t D(1-\nu)\kappa_{2} \end{aligned} \quad , \tag{19}$$

used in the papers [9][10][11][13][12][14][15] follows from expression for elastic energy density assumed as a particular case of (2) (see for example [16])

$$\begin{aligned} 2\Phi(\boldsymbol{\varepsilon}) = C\left[\nu tr^2\boldsymbol{E}_{\|}+(1-\nu)tr(\boldsymbol{E}_{\|}^T\boldsymbol{E}_{\|})\right]+\alpha_s C(1-\nu)\boldsymbol{t}_N^0\boldsymbol{E}\boldsymbol{E}^T\boldsymbol{t}_N^0 + \\ +D\left[\nu tr^2\boldsymbol{K}_{\|}+(1-\nu)tr(\boldsymbol{K}_{\|}^T\boldsymbol{K}_{\|})\right]+\alpha_t C(1-\nu)\boldsymbol{t}_N^0\boldsymbol{K}\boldsymbol{K}^T\boldsymbol{t}_N^0 \end{aligned} \tag{20}$$

where we define

$$C=\frac{Eh}{1-\nu^2},\ D=\frac{Eh^3}{12(1-\nu^2)} \tag{21}$$

Here (21) h is the shell thickness in the reference configuration.

In (19) and (20) α_s denotes the correction factor for transverse shear stress resultants. This coefficient received much attention in the literature. It usually takes on values between $\pi^2/12$ (cf. [22]) and 1 (for instance Lewiński [23] arrived at the value $14/17$).

The second coefficient, namely α_t, is the correction factor for the stress couples within the general, dynamically and kinematically exact, six-field theory of elastic shells. In [24] the values of both α_s and α_t have been established for that theory. Using the complementary energy density derived from the transverse shear stresses acting only on the shell cross section and assuming appropriate quadratic and cubic distributions of the stresses across the thickness, the consistent constitutive equations for the transverse shear stress resultants and stress couples with α_s and α_t as the respective correction factors have been arrived at respectively as

$$\alpha_s=5/6,\ \alpha_t=7/10 \tag{22}$$

The obtained values do not depend on the shell material symmetry, geometry of the base surface, the shell thickness, or any kind of kinematic and/or dynamic constraints.

In [25] it is shown that under some conditions for micropolar material constants in 3D material law and for the curvature energy, upon through-the-thickness integration of expression for elastic energy, there appears constants α_2 that plays the same role as α_t of the present six-field theory. It is argued in [25] that for $\alpha_2>0$ the curvature energy would also depend on the non-symmetric part of the curvature tensor. As a consequence, the

resulting 2D limit energy in Γ convergence would depend on imposed boundary conditions specified, for Cosserat rotation vector.

2.3. Equivalence

As it has been shown in paper [8] the constitutive relations (18) and (19) are equivalent if

$$\alpha_2 = 0 \Leftrightarrow N = \frac{\sqrt{2}}{2} \text{ and } \alpha_t = \frac{2-\nu}{1-\nu} \tag{23}$$

Note that under $(23)_1$ and with $(12)_1$ we have

$$\kappa = 2\mu \frac{N^2}{1-N^2} \Rightarrow \kappa = 2\mu \tag{24}$$

Specifying now relation $(2.14)_2$ from paper [17] i.e.

$$N^2 = \frac{\mu_c}{\mu_c + \mu} \tag{25}$$

for $N = \frac{\sqrt{2}}{2}$ yields

$$N^2 = \frac{\mu_c}{\mu_c + \mu} \Rightarrow \mu_c = \mu \tag{26}$$

which together with (24) identifies μ_c as $\frac{\kappa}{2}$.

Further, rewriting the relation (10) with simultaneous use of (13) yields the relation

$$\beta_3 = 2\mu h\left(2l_b^2 - \tfrac{1}{12}\tfrac{1}{1-\nu}h^2\right) \equiv 2\mu h \tfrac{1}{12} h^2 \tag{27}$$

Additionally, after some manipulations the following relations have been obtained in [1]

$$l_t^2 = \tfrac{1}{6}\tfrac{1}{1-\nu}h, \ \Psi = \tfrac{2}{2+\nu} \tag{28}$$

Substituting formulae (28) and (28) one can show that the terms underlined in (18) disappear yielding exactly the material law (19).

3. Conditioning of constitutive matrix

The issue of conditioning of constitutive matrix has been addressed in [6] (eq. 15). Here we carry out a more detailed study.

It is known, see for instance [26], that $n \times n$ real symmetric matrix is positive definite if all its eigenvalues are positive. In case of (18) the respective formulae for eigenvalues λ_n and eigenvectors $\boldsymbol{v}_n$ are

$$\lambda_1 = -\frac{EhN^2}{(N^2-1)(1+\nu)}, \quad \boldsymbol{v}_1 = [1,1,0,0,0,0,0,0,0,0,0,0]^T \tag{29}$$

$$\lambda_2 = \frac{Eh}{1+\nu}, \quad \boldsymbol{v}_2 = [0,0,1,1,0,0,0,0,0,0,0,0]^T \tag{30}$$

$$\lambda_3 = \frac{Eh}{1+\nu}, \quad \boldsymbol{v}_3 = [-1,1,0,0,0,0,0,0,0,0,0,0]^T \tag{31}$$

$$\lambda_4 = \frac{Eh}{1-\nu}, \quad \boldsymbol{v}_4 = [0,0,0,0,0,0,0,0,0,0,0,1]^T \tag{32}$$

$$\lambda_5 = -\frac{Eh}{2(-1+N^2)(1+\nu)}, \quad \boldsymbol{v}_5 = [0,0,0,0,0,0,0,0,0,0,1,0]^T \tag{33}$$

$$\lambda_6 = -\frac{Eh}{2(-1+N^2)(1+\nu)}, \quad \boldsymbol{v}_6 = [0,0,0,0,0,0,0,0,-1,1,0,0]^T \tag{34}$$

$$\lambda_7 = -\frac{Eh\left(h^2+12(-4l_b^2+l_t^2)\right)}{12(1+\nu)}, \quad \boldsymbol{v}_7 = [0,0,0,0,0,1,0,0,0,0,0,0]^T \tag{35}$$

$$\lambda_8 = \frac{Eh\left(12l_t^2(-1+\nu)+h^2(1+\nu)\right)}{12(1+\nu)}, \quad \boldsymbol{v}_8 = [0,0,0,0,1,0,0,0,0,0,0,0]^T \tag{36}$$

$$\lambda_9 = \frac{Eh\left(12l_t^2(-1+\nu)+h^2(1+\nu)\right)}{12(1+\nu)}, \quad \boldsymbol{v}_9 = [0,0,-1,1,0,0,0,0,0,0,0,0]^T \tag{37}$$

$$\lambda_{10} = -\frac{Eh\left(h^2\Psi(2+N^2(-3+\nu))+12l_t^2(-1+N^2)(-2+\Psi)(-1+\nu)\right)}{12\Psi(-1+N^2)(-1+\nu)(1+\nu)}, \quad \boldsymbol{v}_{10} = [0,0,0,0,0,0,0,0,1,1,0,0]^T \tag{38}$$

$$\lambda_{11} = \frac{2Ehl_b^2}{1+\nu}, \quad \boldsymbol{v}_{11} = [0,0,0,0,0,0,-1,1,0,0,0,0]^T \tag{39}$$

$$\lambda_{12} = \frac{2Ehl_b^2}{1+\nu}, \quad \boldsymbol{v}_{12} = [0,0,0,0,0,0,1,1,0,0,0,0]^T \tag{40}$$

Here the order of eigenvalues does not reflect the growth of their values.

Since N is the real positive constant, to make eigenvalues (29)-(33) positive it is necessary that

$$0 < N < 1 \tag{41}$$

Under the usual assumption that $0 \le \nu \le 0.5$ from (39) one gets

$$l_b^2 > 0 \tag{42}$$

which confirms the physical meaning of $l_b > 0$.

Equations (36) and (37) furnish the condition

$$\lambda_8 = \lambda_9 > 0 \Leftrightarrow 12l_t^2(-1+\nu)+h^2(1+\nu) > 0 \tag{43}$$

From the latter inequality, with given h and ν, follows the explicit condition

$$0 < \frac{h^2}{12}\frac{1+\nu}{1-\nu} < l_t^2 \tag{44}$$

Additionally we obtain

$$\min_{\nu=0} l_t^2 > \frac{h^2}{12}, \quad \max_{\nu=0.5} l_t^2 > \frac{h^2}{4} \tag{45}$$

From the equation (35) it may be inferred that

$$\lambda_7 > 0 \Leftrightarrow h^2 + 12(-4l_b^2 + l_t^2) < 0 \tag{46}$$

Solving the inequality (46) for l_t^2, we obtain the condition

$$l_t^2 < \frac{48l_b^2 - h^2}{12} \tag{47}$$

With (44) and (47) we obtain bounds on l_t^2,

$$\frac{h^2}{12}\frac{1+\nu}{1-\nu} < l_t^2 < \frac{48l_b^2 - h^2}{12} \tag{48}$$

Solving (46) for l_b^2 we obtain restriction (additional to (42)) on values of l_b^2,

$$l_b^2 > \frac{h^2 + 12l_t^2}{48} \tag{49}$$

The precise estimation of the upper bound of l_b^2 remains an open question in this study. Eringen [2] (see Section 5.13) argues that the micropolar effects will be observable when characteristic length will be of the order of plate thickness. Based on their analysis Altenbach and Eremeyev [6] have shown that the micropolar effects are inessential if $0.5h > l_b$. In view of these suggestions we assume that the maximum value of l_b will be taken as equal to the shell thickness h. Thus we arrive at estimation

$$\sqrt{\frac{h^2 + 12l_t^2}{48}} < l_b < h \tag{50}$$

In [27] it has been shown that values of the micropolar ratio Ψ are bounded by

$$0 \le \Psi \le \frac{3}{2} \tag{51}$$

From (51) it follows therefore that the denominator in the equation (38) may take on zero value when $\Psi = 0$ which is impossible. Therefore, in the present approach, the inequality (51) should be modified to

$$0 < \Psi \le \frac{3}{2} \tag{52}$$

In reference [17] it has been shown among others that for the case of conformal bending (see [17] for details) that

$$\Psi = \frac{3}{2} \text{ and } l_t = 2l_b \tag{53}$$

in the case of 3D problems. Obviously the criterion (53) in such a case can not depend on the characteristic dimension, h, of 2D mechanical problems i.e. plates, shells. Here, in (49) h comes in to play naturally.

With restrictions (41) and (52) and with typical values of the Poisson ratio $0 \le \nu \le 0.5$ the denominator of (38) is always positive. Hence, the numerator of (38) should be negative to keep (38) positive. This reasoning furnishes the following inequality

$$f = Eh\left(h^2\Psi(2+N^2(-3+\nu))+12l_t^2(-1+N^2)(-2+\Psi)(-1+\nu)\right)<0 \tag{54}$$

The inequality (54) is linear in Ψ. Let us rewrite (54) in the form

$$f = A\Psi - B < 0 \tag{55}$$

In (55) we have introduced two constants defined as follows

$$A = Eh(2h^2+12l_t^2-3h^2N^2-12l_t^2N^2-12l_t^2\nu+h^2N^2\nu+12l_t^2N^2\nu) \tag{56}$$

$$B = 24Ehl_t^2(-1+N^2)(-1+\nu) \tag{57}$$

Equating (55) to zero and solving for Ψ we obtain the formula

$$\Psi_0 = \frac{24l_t^2(-1+N^2)(-1+\nu)}{2h^2+12l_t^2-3h^2N^2-12l_t^2N^2-12l_t^2\nu+h^2N^2\nu+12l_t^2N^2\nu} \tag{58}$$

Equation (58) establishes the upper bound for values of Ψ within the restriction (51).

Based on the above considerations, we propose the following algorithm for parametric analysis based on the micropolar constants, which furnishes positive definite constitutive matrix. Given E, ν, h and l_b (or l_t) do:

1. Find bounds for l_t from inequalities (48) (or find bounds for l_b through (50))
2. Given N and l_t as established above, find the maximum value of Ψ using (58)

4. Parametric study and numerical example

As an example of shell structure we choose the simply supported channel beam loaded with uniformly distributed load, see [28] and for example [12] (cf. Figure. 1). This shell structure is composed of plates, but at the same time it contains orthogonal intersections. Geometry is described by $L = 36$ in, $a = 2$ in, $b = 6$ in, $h = 0.05$ in. The load is $p = 100$ lb/in while the material constants are $E = 10^7$ lb/in and $\nu = 0.333$. In the nonlinear analysis the evolution of load is controlled by the scalar parameter λ. As in our previous paper [1] in computations we exploit symmetry of the structure. We use 16-node CAM elements (see [10], [12]) with full integration of element matrices and with mesh built of 4 elements for each flange, 8 elements for web and 24 elements for half of the beam.

The study breaks down into three parts. The first part is concerned with the analysis of some selected eigenvalues. Using the restrictions derived above, the functions of λ_1, λ_8, λ_7 and λ_{10} are plotted against their arguments to show that the eigenvalues are positive indeed.

The second part aims at answering the question of influence of variations of the material parameters on variations of some control parameters: elastic energy of the structure and non-zero generalized displacements of the point (a).

The third part of the analysis utilizes the results and conclusions from the first part and is devoted to the geometrically nonlinear analysis.

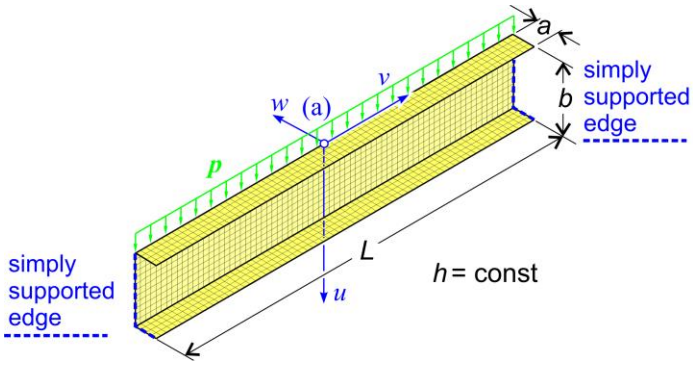

Figure. 1. Simply supported channel beam, geometry and load

4.1. Study on values of λ_p

For the purposes of the subsequent analyses we populate a set $\boldsymbol{Z}_0$ whose elements are material constants

$$\boldsymbol{Z}_{(0)} = \left\{E, \nu, N_{(0)}, l_{b(0)}, l_{t(0)}, \Psi_{(0)}\right\} \tag{59}$$

Utilizing the relations 26 and 33 from the paper [1] i.e.

$$N = \tfrac{\sqrt{2}}{2},\ l_t^2 = \tfrac{1}{6}\tfrac{1}{1-\nu}h,\ \Psi = \tfrac{2}{2+\nu} \tag{60}$$

and

$$2l_b^2 - \tfrac{1}{12}\tfrac{1}{1-\nu}h^2 \equiv \tfrac{1}{12}h^2,\quad l_b^2 = \tfrac{1}{24}\tfrac{2-\nu}{1-\nu}h^2,\quad \tfrac{l_b^2}{h^2} = \tfrac{1}{24}\tfrac{2-\nu}{1-\nu}. \tag{61}$$

we arrive at

$$\boldsymbol{Z}_{(0)} = \left\{10^7; 0.333; \tfrac{1}{2}\sqrt{2}; 0.016135013; 0.024993752; 0.857265324\right\} \tag{62}$$

In (59), E and ν are held fixed. The remaining values are computed assuming the equivalence between the model from [6] and the six-field nonlinear shell theory. Throughout the remaining part of the text we name all the results based on values presented in (62) as the ‘equivalent model”.

With E, ν and h given, the restrictions on micropolar values are as follows. The lower and upper bounds of l_b follow from (50)

$$\frac{h\sqrt{3}}{12} = \frac{0.05\sqrt{3}}{12} = 0.00722 < l_b < 0.05 = h \tag{63}$$

The characteristic length for torsion is then restricted by (48). Using the upper bound $l_b = h$, for the characteristic length for bending we obtain

$$\sqrt{\frac{h^2}{12}\frac{1+\nu}{1-\nu}} = \sqrt{\frac{0.05^2}{12}\frac{1+0.333}{1-0.333}} = 0.02040 < l_t < \sqrt{\frac{48l_b^2 - h^2}{12}} = \sqrt{\frac{48\cdot 0.05^2 - 0.05^2}{12}} = 0.09895 \tag{64}$$

The characteristic length for bending with given l_t is restricted by inequalities (50),

$$\sqrt{\frac{0.05^2 + 12 \cdot 0.024993752^2}{48}} = 0.01443 < l_b < 0.05 \tag{65}$$

With $N = N_{(0)} = \frac{1}{2}\sqrt{2}$, $l_t = 0.024993752$ and through the relation (58) we find that $\Psi_0 = 1.20012$ which is smaller than the maximum admissible value $\Psi = 1.5$. It may now be verified that all the values presented in (62) satisfy their respective limits.

Figure 2 portrays the dependence of λ_1 on N. From equation (29) it follows that λ_1 approaches infinity as we have

$$\lim_{N \to 1} \lambda_1 \to \infty \tag{66}$$

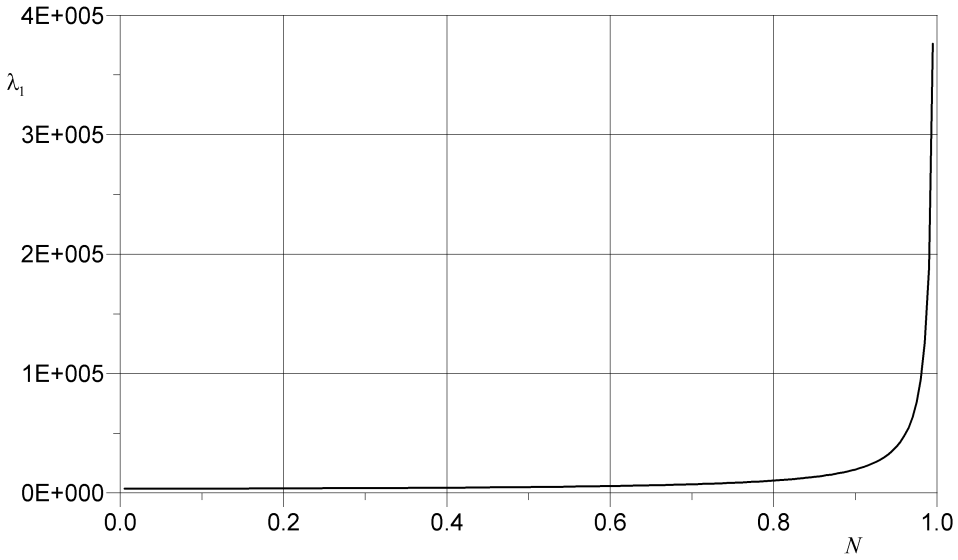

Figure 2. Values of λ_1 versus N

From the equation (36) follows the relation λ_8 versus l_t shown in Figure 3. By making use of inequality (64) Figure 3 depicts the admissible values of l_t as obtained from the equation (36).

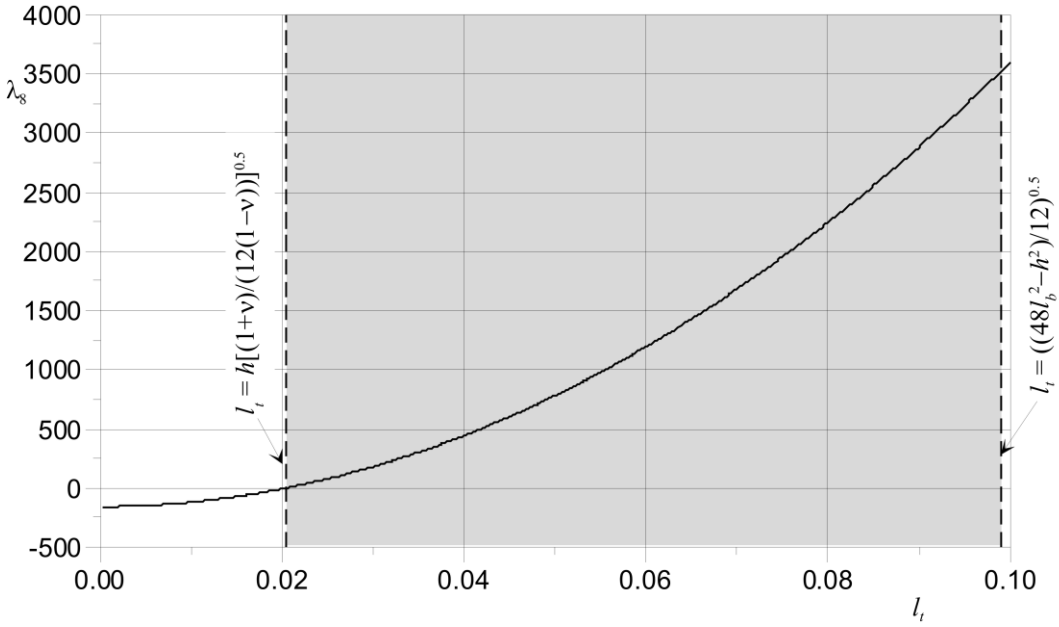

Figure 3. Values of λ_8 versus l_t

The equation (35) represents a surface $\lambda_7 = f(l_b, l_t)$. Figure 4 shows changes of λ_7 versus l_b and l_t. The dashed line in this figure which marks the transition from negative to positive values of λ_7, is found from the right-hand side of inequality (48).

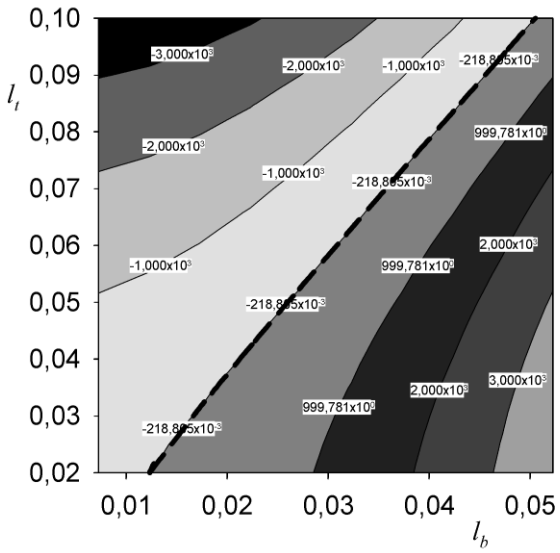

Figure 4. Values of λ_7 versus l_t and l_b

Using (38), the surface λ_{10} is plotted against l_t and $\Psi < \Psi_0$ in Figure 5 for $N = \frac{1}{2}\sqrt{2}$. It is seen that all the values are positive and attain the maximum for small Ψ and large l_t.

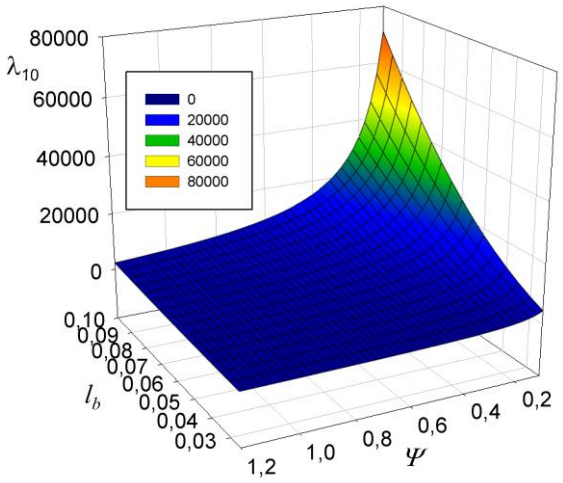

Figure 5. Values of λ_{10} versus l_t and Ψ, $N = 0.1$

4.2. Linear parametric-sensitivity analysis

In this section we perform the linear sensitivity analysis. As the control variables to study we select the total energy of the structure E_{tot}, the horizontal translation of the point (a) $u_{(a)}$, the vertical translation of the point (a) $w_{(a)}$ and the rotation $\phi_{2(a)}$ about y axis at (a). Values of the above control parameters as computed using the values from (62) are as follows

$$[E_{tot}, u_{(a)}, w_{(a)}, \phi_{2(a)}] = [1135.85; 0.19929; 0.19032; -0.12013] \tag{67}$$

Varying the values from (62) within their respective limits, changes of the control variables have been obtained by dividing the computed values by their reference values from (67). For instance, by setting

$$\bar{l}_t = 0.021 \tag{68}$$

we have arrived at the following values

$$[\bar{E}_{tot}, \bar{u}_{(a)}, \bar{w}_{(a)}, \bar{\phi}_{2(a)}] = [1263.29; 0.200784; 0.191668; -0.121708] \tag{69}$$

where the overbar indicates that values in (69) are different from those in (67). Next, by dividing the 'barred' quantities (68) and (69) by appropriate reference values (62) and (67) we have obtained the required normalized change of values of $E_{tot}, u_{(a)}, w_{(a)}, \phi_{2(a)}$. Figure 6 shows the obtained results. The curves are arranged in a way to portray the influence of material parameters $N_{(0)}$, $l_{b(0)}$, $l_{t(0)}$, $\Psi_{(0)}$ on each control parameter. Thereby we are able to detect which of the material parameters plays the dominant role. The curves show significant influence of changes of Ψ and l_t on the solutions, while the variations of l_b yield incomparably smaller variations of the control parameters.

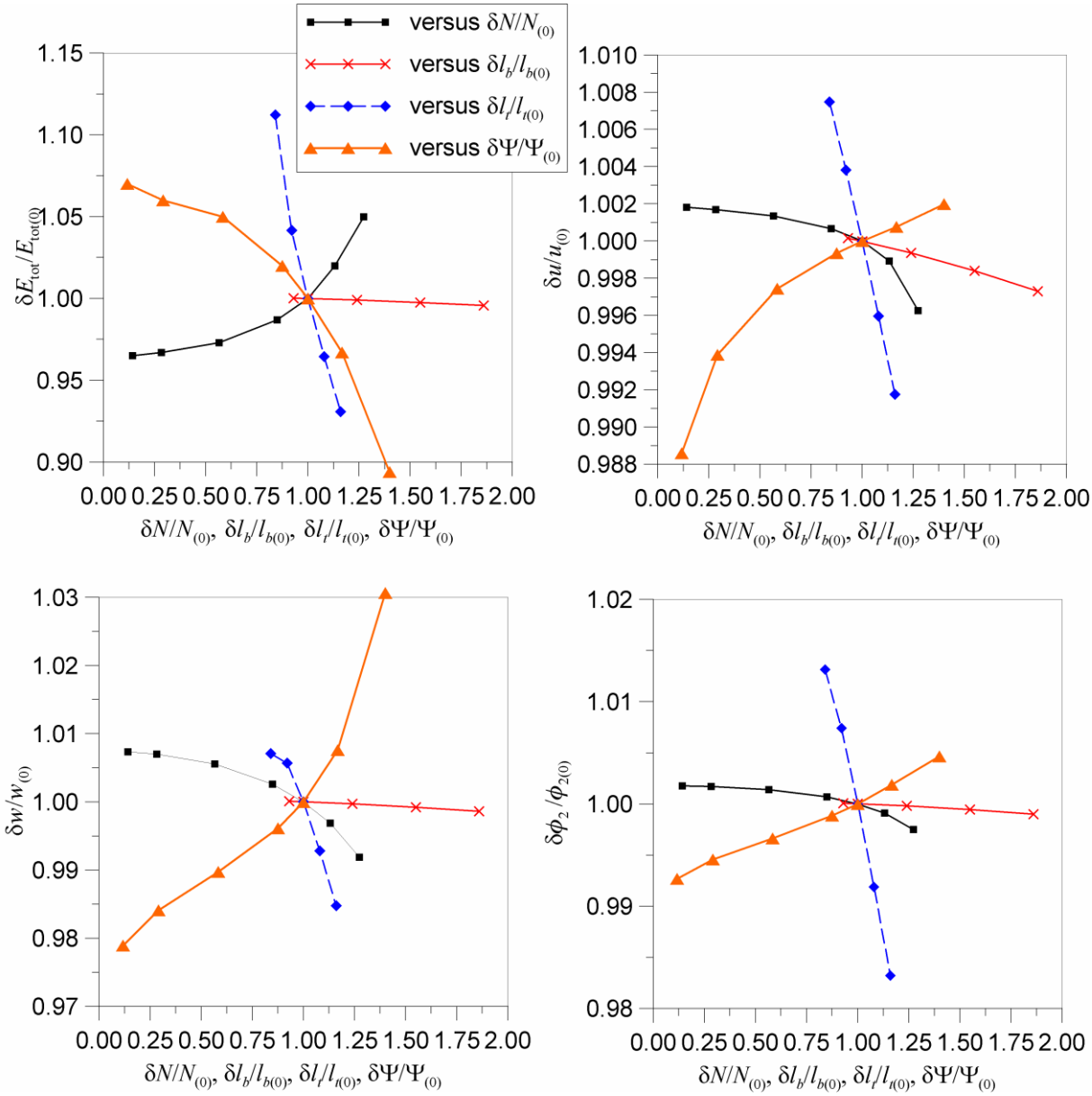

Figure 6. Results of linear sensitivity analysis

4.3. Non-linear analysis

In this section, based on the results of the linear parametric-sensitivity analysis presented above, we discuss the influence of selected micropolar constitutive coefficient on the behavior of the structure in the geometrically non-linear range of deformations. We consider five cases of material parameters. The first one is described by the set (62) and is designated in the text as the 'equivalent model'. In the second and third cases we choose $l_t^{\min} = 0.021$ and $l_t^{\max} = 0.0289875$ of l_t studied in the sensitivity analysis with the remaining values as in (62). Similarly, in the fourth and fifth cases we choose $\Psi^{\min} = 0.1$ and $\Psi^{\max} = 1.2$. All the cases describe in fact different materials. We compare the results not only in terms of overall structural deformation, described by the load-displacement path, but also in terms of computational costs. In the latter case we select the number of iterations required to satisfy convergence criteria. All the examples have been calculated on the same PC with the same arc-length parameters.

Figure 7 depicts the comparison of load-deformation path of translation u of the point (a). For $l_t^{\min} = 0.021$ the curve has some turns shown in detail in Figure 8. It is seen that for this value of $l_t^{\min}$ the path performs multiple turns and is difficult to follow. In the same range of λ and l_t the remaining curves have almost linear character. This is shown in Tab. 1, where results of the linear analysis are shown. The results show that in this range the differences are almost indistinguishable. In brackets we report the relative error with respect to values obtained in the equivalent model

$$error = \frac{(\ldots) - (\ldots)_{equivalent}}{(\ldots)_{equivalent}} \cdot 100\% \tag{70}$$

Table 1. Results of linear numerical calculations, non-zero generalized displacements of point (a)

		E_{tot}	$u_{(a)}$	$w_{(a)}$	$\phi_{2(a)}$
$\Psi = 0.857265324$	$l_t^{\min} = 0.021$	1263.29 (11.22%)	0.200784 (0.75%)	0.191668 (0.71%)	–0.121708 (1.31%)
	$l_t^{\max} = 0.0289875$	1057.22 (–6.92%)	0.197649 (–0.82%)	0.187425 (–1.52%)	–0.18114 (50.78%)
$l_t = 0.024993752$	$\Psi^{\min} = 0.1$	1211.10 (6.62%)	0.197016 (–1.14%)	0.186312 (–2.11%)	–0.19252 (60.25%)
	$\Psi^{\max} = 1.2$	1016.00 (–10.55%)	0.199686 (0.20%)	0.196157 (3.06%)	–0.20689 (72.22%)
	Equivalent model (reference)	**1135.85**	**0.199288**	**0.190324**	**–0.120134**

Tab. 1 shows that the micropolar material parameters influence significantly the total energy of the structure and the rotation $\phi_{2(a)}$. It indicates that there may appear some deformation patterns involving different deformation waves. This fact is discussed later in this paper.

The costs of the solutions measured by the number of iterations are presented in Figure 9 for the equivalent model and in Figure 10. For $l_t^{\min} = 0.021$ the number of iterations varies rapidly with the maximum number of iterations equal to 16, while in the remaining cases the number of iterations is almost constant.

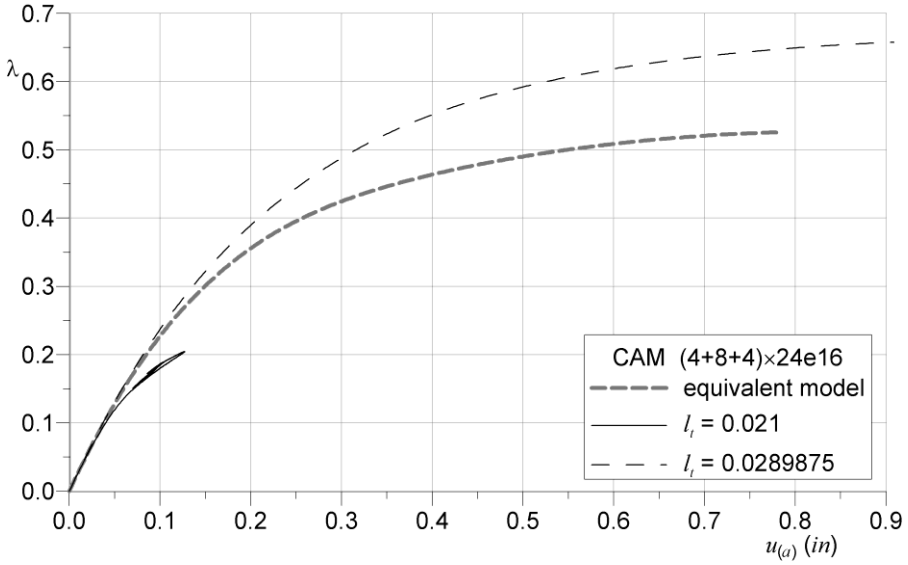

Figure 7. Results of non-linear analysis, changes of l_t

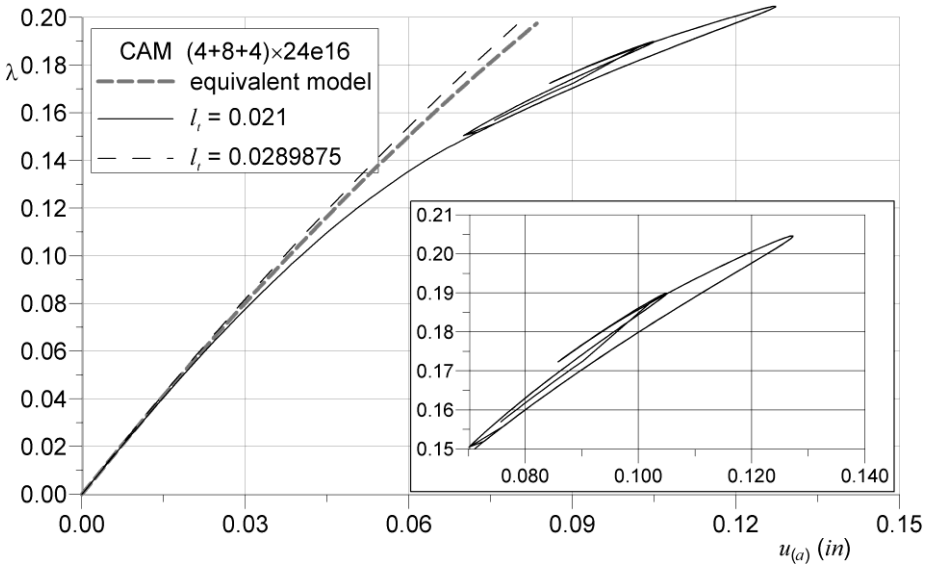

Figure 8. Results of non-linear analysis, changes of l_t, details

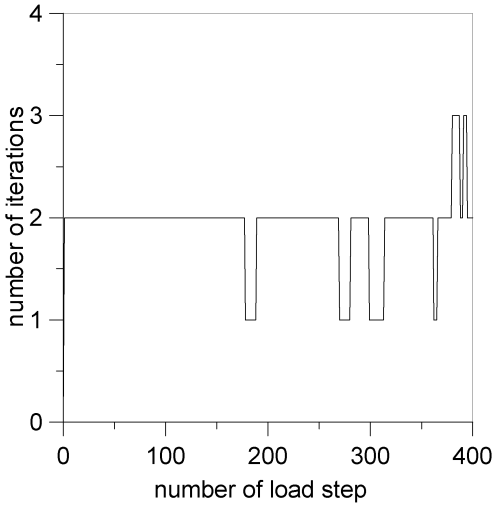

Figure 9. Number of iterations in the equivalent model

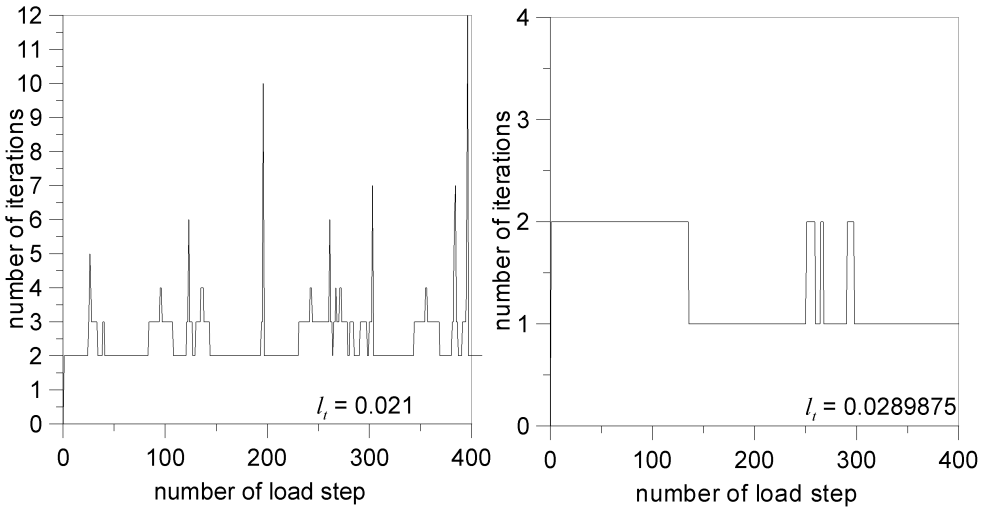

Figure 10. Number of iterations for $l_t^{\min}$ (left) and $l_t^{\max}$ (right)

The influence of $\Psi^{\min} = 0.1$ and $\Psi^{\max} = 1.2$ on the values of translation u of the point (a) is portrayed in Figure 11, while some details are shown in Figure 12. In this case the most complicated response appears if $\Psi^{\max} = 1.2$.

To throw some light on possible deformed configurations, Fig. 14 portrays deformed the meshes obtained for values of the control translation $u_{(a)}$ close to 0.034 using different values of l_t. To amplify differences the meshes are scaled by the factor 5. It is seen that when l_t approaches its lower bound 0.02040 local forms of stability loss appear on the lower flange. In case of two remaining values of l_t studied here such effects do not appear. This explains the complicated nature of the load-deformation path from Figure 8.

Figure 15 depicts somewhat different responses. Here $u_{(a)}$ is close to 0.35 and the response of the structure is compared for different values of Ψ. The range of deformation is large enough to compare it with the undeformed mesh without additional magnifications. The graphs show that with the growth of Ψ the response of the structure changes considerably. When $\Psi = 0.1$ the beam deforms without deformation of the cross-section. With the growth of Ψ, however, the beam exhibits deformations involving significant deformations of the cross-section with simultaneous propagation of deformation waves.

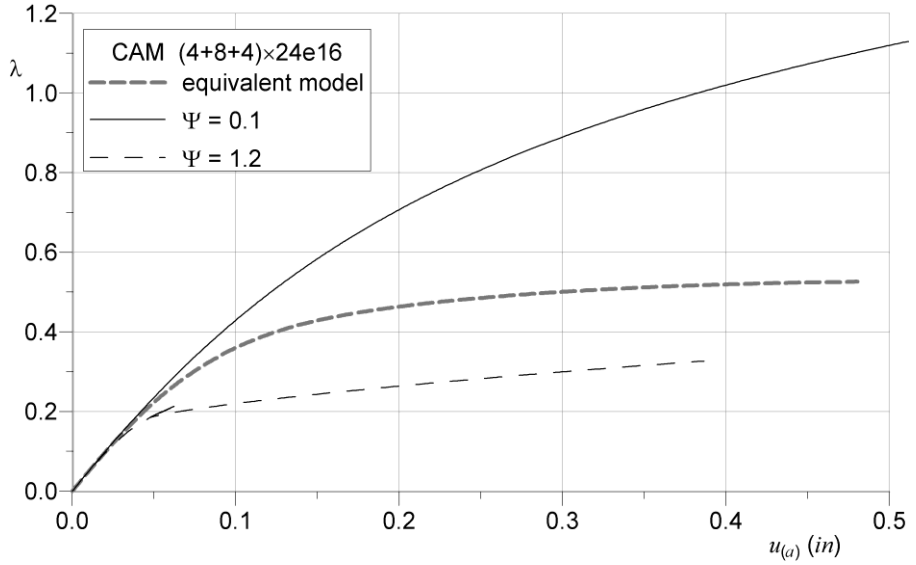

Figure 11. Results of non-linear analysis, changes of Ψ

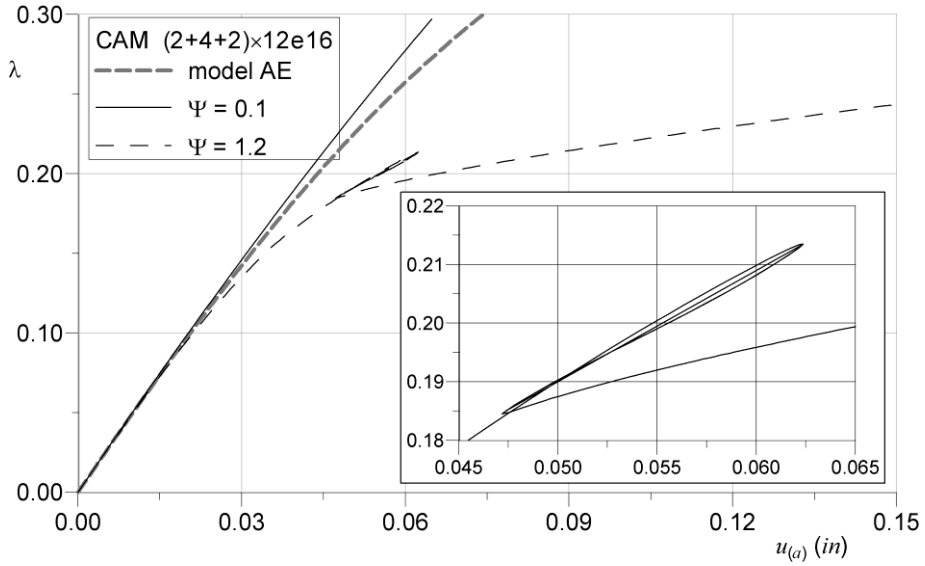

Figure 12. Results of non-linear analysis, changes of Ψ, details

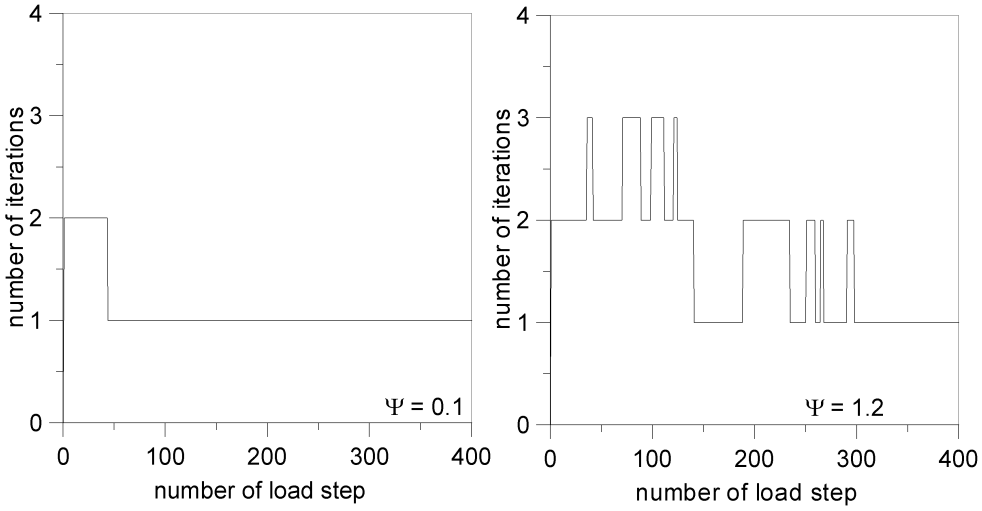

Figure 13. Number of iterations for $\Psi^{\min} = 0.1$ (left) and $\Psi^{\max} = 1.2$ (right)

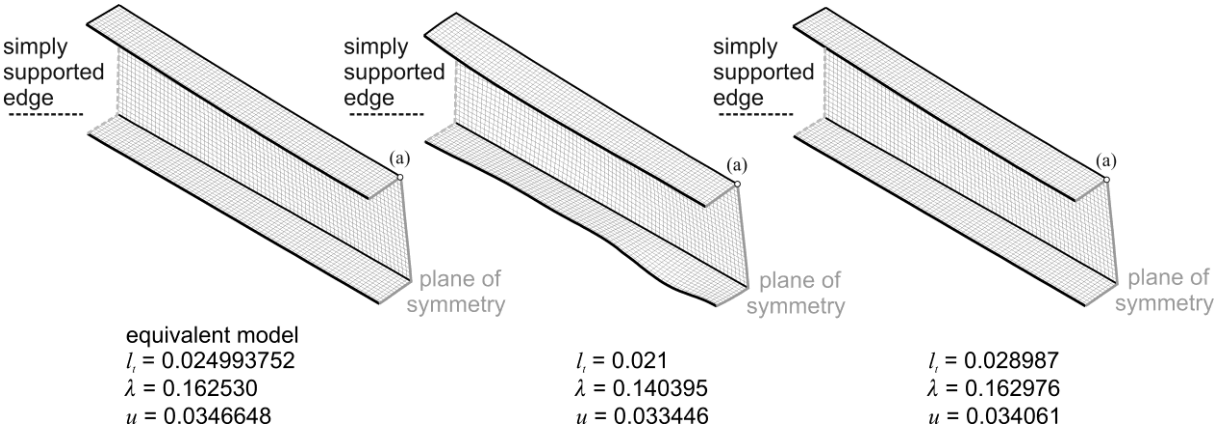

Fig. 14. Deformed meshes for different values of l_t

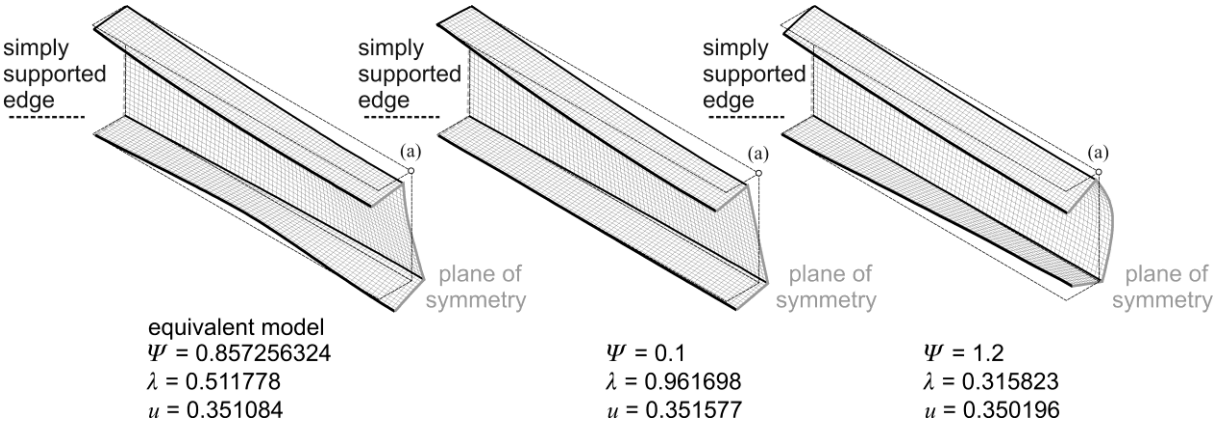

Figure 15. Deformed meshes for different values of Ψ

5. Conclusions

In this paper we have estimated the bounds for values of the micropolar material constants within the model of Cosserat plates of Altenbach and Eremeyev [6]. We have shown that an inappropriate selection of the micropolar constants may yield a non-positive definite constitutive matrix, so these constants should obey some limitations that we have derived. We have proposed some algorithm to establish these bounds.

However, the present study does not provide any suggestions for to explicit values of limits of the material constants. In our methodology these can be established only for a given shell structure with given thickness h, Young's modulus E and Poisson ratio ν. In particular the upper limit of characteristic length for bending l_b cannot be established. We also assume that E and ν have the same character for both Cauchy and Cosserat continuum.

For shell structure in the form of channel section we have performed linear parametric-sensitivity analysis and established dominant parameters in sense of their influence on changes of some control variables. We have also assessed how some material parameters affect the nonlinear response of the structure. Our results show that within the linear analysis differences in values of the displacements and the total energy of the structure are insignificant, regardless of the material parameters used. However, in the nonlinear analysis the differences are

clearly pronounced. This observation may serve as some guidance for the experimental studies on micropolar constants, namely that such experiment should be performed in the nonlinear range of shell deformation.

Acknowledgements: The financial support from the Polish Ministry of Science and Higher Education is acknowledged (grant no. N N506 254237).

References

[1] E. Cosserat, F. Cosserat, Théorie des corps déformables. Librairie Scientifique A. Hermann et Fils (engl. Translation by D. Delphenich 2007, pdf available at http://www.mathematik.tu-darmstadt.de/fbereiche/analysis/pde/staff/neff/patrizio/Cosserat.html), reprint 2009 by Hermann Librairie Scientifique, ISBN 978 27056 6920 1, Paris, 1909.

[2] A.C. Eringen, Microcontinuum Field Theories I, Foundations and Solids. Springer, 1999.

[3] W. Nowacki, Theory of asymmetric elasticity, Pergamon Press, Oxford, 1986.

[4] J. Altenbach, H. Altenbach, V.A. Eremeyev, On generalized Cosserat-type theories of plates and shells: a short review and bibliography. Archive of Applied Mechanics, **80**, 73-92 (2010)/DOI: 10.1007/s00419-009-0365-3.

[5] W. Pietraszkiewicz, V.A. Eremeyev, On natural strain measures of the non-linear micropolar continuum, International Journal of Solids and Structures **46**, 774–787 (2009)

[6] H. Altenbach and V. A. Eremeyev, On the linear theory of micropolar plates. Z. Angew. Math. Mech. **89**(4), 242–256 (2009)/DOI 10.1002/zamm.200800207.

[7] S. Ramezani, R. Naghdabadi, Micropolar hypo-elasticity. Archive of Applied Mechanics, DOI 10.1007/s00419-010-0466-z.

[8] J. Chróścielewski and W. Witkowski, On some constitutive equations for micropolar plates. Z. Angew. Math. Mech. **90**(1), 53–64 (2010)/DOI 10.1002/zamm.200900366

[9] A. Libai and J.G. Simmonds, The Nonlinear Theory of Elastic Shells, 2nd edn. Cambridge University Press, Cambridge, 1998.

[10] J. Chróścielewski, J. Makowski and H. Stumpf, Genuinely resultant shell finite elements accounting for geometric and material non-linearity, International Journal for Numerical Methods in Engineering, **35**, 63–94 (1992).

[11] J. Chróścielewski, J. Makowski and H. Stumpf, Finite element analysis of smooth, folded and multi-shell structures, Comp. Meth. Appl. Mech. Engng. **41**, 1–46 (1997).

[12] J. Chróścielewski, J. Makowski and W. Pietraszkiewicz, Statics and Dynamics of Multifold Shells: Nonlinear Theory and Finite Element Method, Institute of Fundamental Technological Research Press, Warsaw, 2004 (in Polish).

[13] J. Chróścielewski and W. Witkowski, 4-node semi-EAS element in 6–field nonlinear theory of shells, International Journal for Numerical Methods in Engineering, **68**, 1137–1179 (2006)/DOI: 10.1002/nme.1740.

[14] J. Chróścielewski and W. Witkowski, Discrepancies of energy values in dynamics of three intersecting plates, Int. J. Numer. Meth. Biomed. Engng. **26**, 1188–1202 2010 (2008)/DOI: 10.1002/cnm.1208 (Commun. Numer. Meth. Engng.)

[15] W. Witkowski, 4-Node combined shell element with semi-EAS-ANS strain interpolations in 6-parameter shell theories with drilling degrees of freedom, Computational Mechanics, **43**, 307–319 2009, DOI 10.1007/s00466-008-0307-x

[16] V. A. Eremeyev and W. Pietraszkiewicz, Local symmetry group in the general theory of elastic shells, J. Elast. **85**(2), 125–152 (2006).

[17] P. Neff, J. Jeong, A. Fischle, Stable identification of linear isotropic Cosserat parameters: bounded stiffness in bending and torsion implies conformal invariance of curvature, Acta Mechanica, 211, 237-249 (2010)/DOI: 10.1007/s00707-009-0230-z

[18] R.D. Gauthier and W.E. Jahsman, A quest for micropolar elastic constants. J. Applied Mechanics, **42**, 369–374 (1975)

[19] R.D. Gauthier andW.E. Jahsman, A quest for micropolar elastic constants, part II. Arch. Mech., **33**, 717–737 (1981).

[20] S. C. Cowin, An incorrect inequality in micropolar elasticity theory, J. Appl. Mech. Phys., **21**, 494–497 1970.

[21] W. Nowacki, Couple-stresses in the theory of thermoelasticity. W: Irreversible aspects of continuum mechanics and transfer of physical characteristics in moving fluids. IUTAM Symposia Vienna 1966. Ed. H. Parkus; L. I. Sedov. Wien: Springer-Verlag, 1968, s. 259–278, pdf available at http://bcpw.bg.pw.edu.pl/Content/970/IUTAM_Symposia_Vienna_1966_str259_278.pdf)

[22] R. D. Mindlin, Influence of rotatory inertia and shear on flexular motions of isotropic elastic plates, J. Appl. Mech., **18**, 31-38 (1951).

[23] T. Lewiński, On refined plate models based on kinematical assumptions, Ingenieur-Archiv, **57**, 133-146 (1987).

[24] W. Pietraszkiewicz, J. Chróścielewski, W. Witkowski, On shear correction factors in the non-linear theory of elastic shells, International Journal of Solids and Structures, accepted for publication, DOI No:10.1016/j.ijsolstr.2010.09.002.

[25] P. Neff, K-I. Hong, J. Jeong, The Reissner-Mindlin plate is the Γ-limit of Cosserat elasticity. Mathematical Models and Methods in Applied Sciences, accepted for publication, DOI No: 10.1142/S0218202510004763

[26] G.A. Korn and T.M. Korn, Mathematical handbook for scientists and engineers. Definitions, theorems and formulas for reference and review. Dover Publications, Inc, Mineola, New York 2000.

[27] P. Neff, The Cosserat couple modulus for continuous solids is zero viz the linearized Cauchy-stress tensor is symmetric. Z. Angew. Math. Mech. **86**(11), 892–912 (2006) / DOI 10.1002/zamm.200510281.

[28] H.P. Lee and P.J. Haris, Post-buckling strength of thin-walled members. Computers & Structures, **10**, 689-702 (1979).